6th European Conference on Computational Mechanics (ECCM 6)
7th European Conference on Computational Fluid Dynamics (ECFD 7)
1115 June 2018, Glasgow, UK

DEVELOPMENT OF AN IMPULSE–SOURCE–BASED WAVE-CURRENT INTERACTION MODEL

CHRISTIAN WINDT[1,2], JOSH DAVIDSON[3], PÁL SCHMITT[4] AND JOHN V. RINGWOOD[1]

[1] Centre for Ocean Energy Research
Maynooth University, North Campus, Ireland
[2] christian.windt.2017@mumail.ie

[3] Department of Fluid Mechanics, Faculty of Mechanical Engineering
Budapest University of Technology and Economics, Hungary

[4] Marine Research Group
Queen's University Belfast, UK, BT9 5AG Belfast, Northern Ireland

Key words: wave-current interaction, impulse source wave maker, internal wave maker, numerical wave tank

Abstract. The analysis of wave-current interaction (WCI) in numerical wave tanks (NWTs) requires the simultaneous generation of a current velocity profile and free surface waves. This paper presents a novel approach to simulate the WCI using an impulse–source–based methodology together with a numerical beach implementation. Three additional terms are added to the momentum equation, to incorporate current and wave generation, as well as the numerical beach. The model components, i.e. wave and current generation, and WCI, are verified independently against two sets of reference data [1, 2]. The results show excellent agreement for the wave-only case, while for the current-only and thus WCI, some model weaknesses can be identified.

1 INTRODUCTION

The interaction between waves and currents is a common problem in the ocean and marine engineering sector. A first description of wave-current interaction (WCI) was delivered by [3]. Since then, numerous studies have been performed using different analysis tools ranging from analytical descriptions to experimental tank testing and numerical models. The main analysis tool used to date is scaled experimental tank tests [4, 5, 6, 7, 8]. Such tests are prone to scaling effects, undesired influences of measurement equipment and test environment, and significant costs. In times of increasing computational power, CFD-based numerical wave tanks (CNWT) are a viable alternative to experimental tank tests, avoiding the aforementioned problems. However few CNWTs models able to simulate WCI have been described in literature [9]-[13].

This study presents an impulse–source–based WCI model for CNWTs. Waves and currents are simultaneously generated through the inclusion of source terms, added to the Reynolds Averaged Navier-Stokes (RANS) equations. Wave generation is based on the implementation presented in [14]. The constant current is generated and controlled through another impulse correction term.

Results are presented for wave-only, current-only and WCI simulations. For verification purposes, the results will be compared to literature benchmark cases [1] and [2].

The remainder of the paper is organised as follows. Section 2 describes the implementation of the additional source terms in the impulse equation and the setup of the numerical wave-current tank is explained. Following, the case study used as benchmark for the verification is described in Section 3. The results of this verification study are presented and discussed in Section 4. Finally, conclusions are drawn in Section 5.

2 INTERNAL WAVE AND CURRENT GENERATION

A RANS model includes the following impulse equation:

$$\frac{\partial(\rho\mathbf{U})}{\partial t} + \nabla\cdot(\rho\mathbf{U}\mathbf{U}) = -\nabla p + \nabla\cdot\mathbf{T} + \rho\mathbf{F}_b \tag{1}$$

where t is time, $\mathbf{U}$ the fluid velocity, p the fluid pressure, ρ the fluid density, $\mathbf{F}_b$ the external forces such as gravity, and the viscous stress tensor $\mathbf{T} = \mu\nabla^2\mathbf{U} + \frac{1}{3}\nabla(\nabla\cdot\mathbf{U})$, with the dynamic viscosity μ. To implement the impulse sources for wave and current generation, as well as a numerical beach for wave absorption, three terms are added to Eq. (1):

- $r_w\rho\mathbf{a}_{wm}$: This is the source term used for wave generation, where r_w is a binary scalar variable that defines the wavemaker region and $\mathbf{a}_{wm}$ is the acceleration input to the wavemaker at each cell centre within $r_w = 1$. This term is based on the implementation of an internal wavemaker in [14].

- $r_c\rho\,\frac{\mathbf{U_t}-\mathbf{U}}{\Delta t}$: This is the source term used for current generation, where r_c is a binary scalar variable that defines the current generation region. At each cell centre within $r_c = 1$, the acceleration input is defined through the difference between the velocity field $\mathbf{U}$ and a target velocity field $\mathbf{U_t}$.

- $s\vec{n}_z\rho\mathbf{U}$: This describes a dissipation term used to implement a numerical beach, where the variable s, with unit $[\mathrm{s}^{-1}]$, controls the strength of the dissipation [15]. Compared to the implementation in [14] and [15], in this study the beach only acts in the vertical, z-direction, to dissipate the waves, while allowing for a steady current flow in x-direction.

Augmenting Eq. (1) with these three terms yields the adapted impulse equation:

$$\frac{\partial(\rho\mathbf{U})}{\partial t} + \nabla\cdot(\rho\mathbf{U}\mathbf{U}) = -\nabla p + \nabla\cdot\mathbf{T} + \rho\mathbf{F}_b + r_w\rho\mathbf{a}_{wm} + r_c\rho\,\frac{\mathbf{U_t}-\mathbf{U}}{\Delta t} + s\vec{n}_z\rho\mathbf{U} \tag{2}$$

2.1 Numerical wave and current tank

To generate a superimposed wave and current field, two separate source regions for wave and current generation have to be defined. Furthermore, the two source regions should be separated by numerical beaches, to eliminate any wave velocity from entering the current source region, which would interfere with the calculation of the current source term required to ensure a constant current-velocity profile. A schematic of the tank layout, position of the different source regions and the numerical beach, is depicted in Figure 1.

To enable a constant current flow in the domain, cyclic boundary conditions (BCs) are used at the inflow and outflow boundaries of the numerical domain. For the top and bottom boundaries of the domain, no slip wall boundaries are used. To reduce the required time for flow development, the whole domain can be initialised with the desired horizontal velocity field. In this initial study of the WCI using impulse sources, all simulations are performed in a pseudo two-dimensional domain, i.e. one cell thickness. A minimum cell size of 10 cells per wave height, with a maximum aspect ratio of 2 and 4, is set in the free surface region and in the vicinity of the bottom wall, respectively.

While the current source strength is internally adapted during the simulation, based on the difference between the desired and instantaneuos current velocity, the input for the wave source is defined *a priori*, requiring preliminary calibration runs [14]. For the numerical beach, the dissipation strength is gradually increased over the beach length ℓ, following Eq. (3).

$$s(x) = -2 \cdot s_{max} \left(\frac{(\ell - x)}{\ell} \right)^3 + 3 \cdot s_{max} \left(\frac{(\ell - x)}{\ell} \right)^2 \tag{3}$$

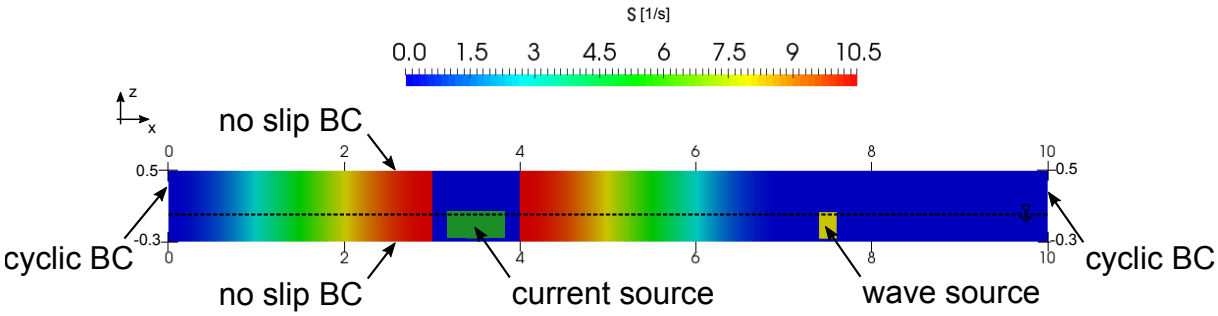

Figure 1: Positioning of the numerical beach, the current and wave source in the numerical wave-current tank

3 CASE STUDIES

To verify the internal wave and current generator proposed in this paper, three case studies are considered: wave-only, current-only, and then WCI simulations. The wave-only simulations are compared against experimental data from [16] and results from the numerical study by Zhang et al. [2]. Zhang et al. considers waves of period $T = 1$s and heights $H = \{0.010\text{m}, 0.023\text{m}, 0.0361\text{m}\}$. The water depth is set to $d = 0.3$m, yielding a wave length $\lambda = 1.372$m according to the linear dispersion relation. The WCI simulations are also compared against the results from [2] and [16], considering the same waves in combination with a uniform, constant current of $U_t = 0.08\text{m}\,\text{s}^{-1}$. Unfortunately, [2] does not provide data for the current-only case, so comparison is made against experimental data from [18] and results from the numerical study by Teles et al. [1]. Teles et al. considers a uniform, constant discharge of $80\text{L}\,\text{s}^{-1}$ ($= U_t = 0.16\text{m}\,\text{s}^{-1}$) in a 0.5m deep tank. A $k - \epsilon$ turbulence model is used throughout the present study.

4 RESULTS AND DISCUSSION

4.1 Preliminary studies

In a preliminary study, the input for the wave impulse source is determined through linear-scaling calibration. A time trace snippet for a_{ana}, where $\mathbf{a}_{wm} = [a_{ana}\ 0\ 0]^T$, is shown in Figure 2. The source length and height, as well as the position, are based upon the parameters presented in [14], i.e. source height d, source length 0.15λ and the source centre is positioned $1/3\,d$ below the still water level.

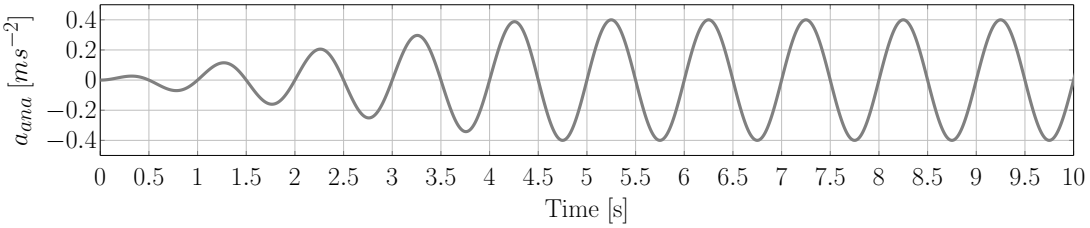

Figure 2: Source input a_{ana} for wave generator

Furthermore, the maximum beach strength s_{max} and beach length ℓ are determined through parametric studies, with the goal of minimising/eliminating wave reflection. Guidance for the selection of s_{max} and ℓ can be found in [14] and [19]. Ultimately, s_{max} is set to 10.5s^{-1} and $\ell \approx 2\lambda$.

For the current source, a parametric study on the source region dimensions has been performed. The final dimensions are $0.8m$ x $0.325m$, for the source length and height, respectively. The centre of the current source region is placed at $0.42d$ below the free surface. To avoid undesired acceleration of the air phase, the current source only marginally pierces the still water line. To prevent violation of the no-slip condition and potential divergence in the turbulence model, a gap between the bottom boundary and current source region of $0.013m$ is kept.

4.2 Wave-only

First, results for the wave-only case are compared to the numerical and experimental data presented in [2].

The impulse source wavemaker has already been verified against wave theory in [14, 20]. In this study, the simulation results are compared to experimental and numerical reference data. Figure 3 shows the free surface elevation, averaged over 15 consecutive periods ($40s \leq \text{Time} \leq 55s$) at two different locations: a) at the centre position of the current source, i.e. 3.5m; b) at a position downstream of the current and wave source, i.e. 9.5m.

At the centre location of the current source, zero surface elevation is desired, so that the input impulse term for the current is not biased by parasitic wave velocity. As in Figure 3 a), this is successfully achieved. At the evaluation location, i.e. $x = 9.5$m, the wave field should accurately recreate the desired wave field. As shown in Figure 3 b), the numerical results from the present study match well with both the experimental and numerical reference data.

Figure 4 shows the horizontal, x-velocity, measured along the depth of the water column, again at the two different locations $x = 3.5$m (Figure 4 a)) and $x = 9.5$m (Figures 4 b) and c)). Furthermore, at the evaluation location, velocities are measured for time instances coincident with a wave crest (b)) and a wave trough (c)). The results are the averaged velocities over 15 consecutive crests/troughs.

Figure 4 a) shows that the horizontal velocity component at the centre location of the current source is zero throughout the simulation, confirming the results in Figure 3 a) that the waves have been succesfully absorbed by the beach before entering the current source region.

At the evaluation location, the horizontal velocities, both at wave crests and troughs, should recreate the desired velocity field. At the wave crest, Figure 4 b) shows very good agreement between the experimental data and the numerical reference. As for the surface elevation results, in general the impulse source wavemaker is able to recreate the desired velocity field more accurately than the methodology employed in the reference study. However, considerably larger deviations can be observed close to the free surface.

At the wave trough, results from the present study coincide with the numerical reference for $-0.25 \leq z/d \leq -1$. Compared to the experimental data, the current implementation and the numerical reference model [2] show noticeable differences for $-0.5 \leq z/d \leq -0.75$. However, since both numerical models are able to recreate the velocity field at the wave crest and coincide for $-0.25 \leq z/d \leq -1$, it can be assumed that inaccuracies in the experimental measurements lead to the mismatch between the data sets. As for the wave crest, larger deviations between experimental and numerical reference data can be observed closer to the free surface, i.e. $0 \leq z/d \leq -0.2$.

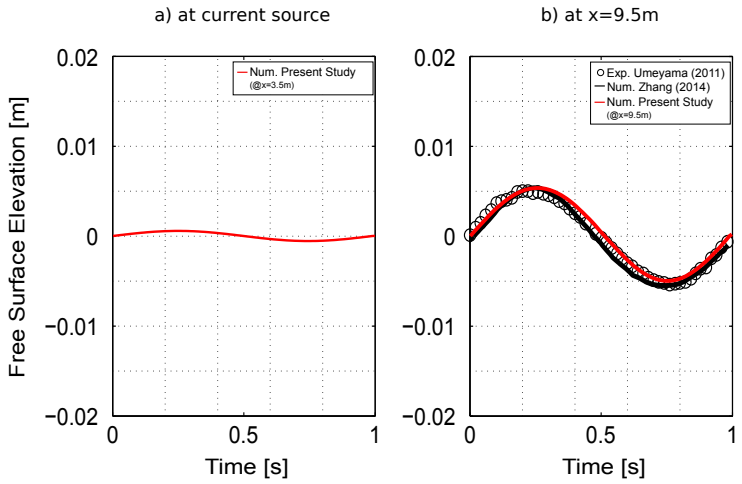

Figure 3: Free surface elevation for the wave only tests case, comparing experimental data (o) [16], numerical data by Zhang et al. [2] and numerical results from the present study

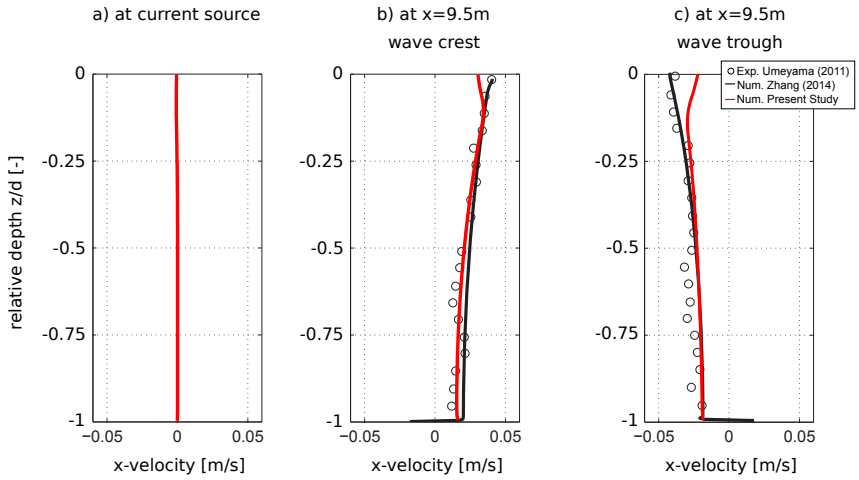

Figure 4: Horizontal x-velocities for the wave only tests case, comparing experimental data (o) [16], numerical data by Zhang et al. [2] and numerical results from the present study

4.3 Current-only

To test the capability of the proposed method to generate a steady current stream, current-only simulations are performed. Since the reference case in [2] does not provide data for current-only cases, results from [1] are used to verify the functionality of the current generator. For these cases, the wave source has been disabled, while the vertically acting beach is still in place. The simulation is initialised with a horizontal velocity of $0.15m/s$, throughout the whole numerical domain, slightly less than the target velocity of $0.16m/s$.

The horizontal velocities at the evaluation point $x = 9.5$m, over the time range $10s \leq t \leq 100s$, are shown in Figure 5. The results show that a steady state current flow is only established after $40s$. Furthermore, over time, the wall boundary layer on the

tank floor increases. For $t > 40s$, the x-velocity decreases with depth in the region $-0.75 \geq z/d \geq -1$, but remains fairly constant in the water column above this, with a velocity of $\approx 0.165m/s$. This maximum steady state velocity is slightly higher than the desired target velocity $0.16m/s$.

Figure 6 also shows the horizontal x-velocity profile generated with the proposed impulse current generator at the evaluation location, at the single time instant, $t = 100$. Additionally, Figure 6 contains numerical and experimental data [1, 18]. Comparing the results from the present study to both, the experimental and numerical reference, a good agreement close to the bottom boundary ($-1 < z/d < -0.85$) can be observed. Also, towards the free surface ($-0.35 < z/d < 0$), a reasonable match is found. However, for ($-0.85 < z/d < -0.35$) relatively large deviations between the results from the present study and the reference data can be observed.

At the time of writing, the source for this mismatch is unknown. It is assumed that the use of wall-functions in the employed implementation of the $k - \epsilon$ turbulence model may affect the numerical results. Also, no error bars on the experimental results are provided, so that the influence of the measurement uncertainty cannot be taken into account, when analysing the fit between the numerical and experimental reference data.

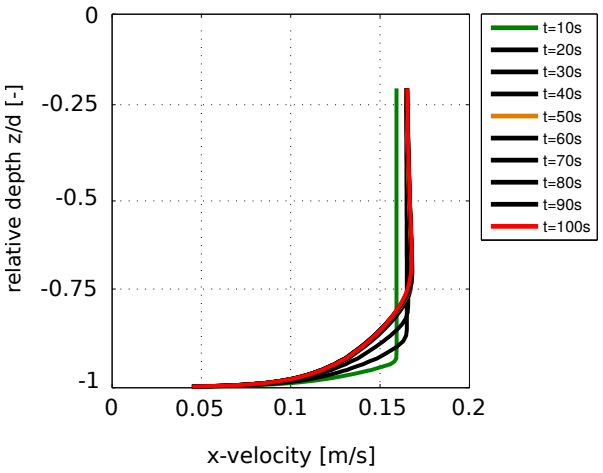

Figure 5: Current-only tests case based on [1]: Horizontal x-velocities at the evaluation location $x = 9.5$m at different time instances $10s \leq t \leq 100s$

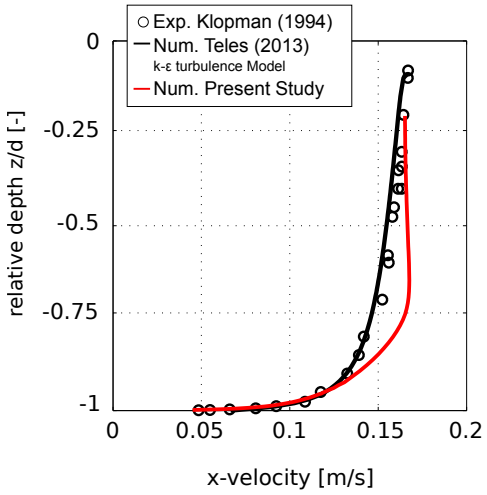

Figure 6: Horizontal x-velocities at the evaluation location $x = 9.5$m at $t = 100s$: Comparing experimental data (o) [18], numerical data by Teles et al. [1] and numerical results from the present study

4.4 Wave-current interaction

As shown in Figure 5, transient behaviour of the current velocity profile can be observed. To eliminate any influence of this transient flow development from the WCI investigation, a current-only case is simulated for the reference case in [2], to determine the time at which steady-state results are achieved. For these cases, the wave source has been disabled, while the vertically acting beach is still in place. At the beginning of the

simulation, a horizontal velocity of $0.06m/s$ is initialised the complete numerical domain.

The horizontal velocities at the evaluation point $x = 9.5$m, over the time range $5s \leq t \leq 200s$, are shown in Figure 7. The results reveal that a steady state current flow is only established after $100s$. For $t > 100s$, the x-velocity decreases with depth in the region $-0.75 \geq z/d \geq -1$, but remains fairly constant in the water column above this, with a velocity of $\approx 0.086m/s$. Hence, for the verification of the WCI, surface elevation data are averaged over 20 consecutive periods between $100s \leq$ Time $\leq 120s$.

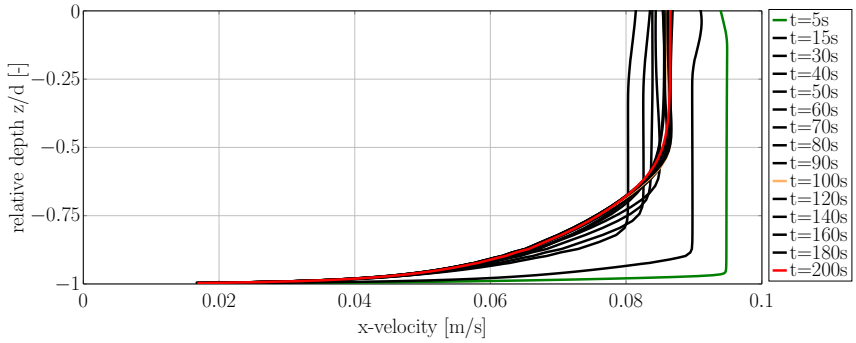

Figure 7: Current-only tests case as in [2]: Horizontal x-velocities at the evaluation location $x = 9.5$m at different time instances $5s \leq t \leq 200s$

Figures 8 and 9 show WCI results for the free surface elevation and velocity profile, respectively. Figure 8 a) includes the experimental data from [16], numerical data from [2] and numerical results from the present study. Figures 8 b) and c) show the difference between the wave-only and WCI case, for the present study and the reference numerical results, respectively. Compared to the experimental data, the presented implementation of the WCI methodology shows a relatively good fit and the start and end of each period. For $0.25s \leq t \leq 0.75s$, larger deviations are observed. The numerical data under-predict the measured surface elevation.

Comparing the numerical data from the wave-only and WCI case gained from the present model, a decrease in the amplitude of the wave can be observed for the WCI case. Also the wave phase is influenced by the current, shifting the trough of the wave. Comparing data from the wave-only and WCI case for the numerical reference case, the decrease in wave amplitude and the phase shift can also be observed, but to a greater extend.

Figure 9 shows the horizontal x-velocity at the evaluation location ($x = 9.5m$) for the wave crest (Figure 9 a)) and trough (Figure 9 b)). As for the wave only case, numerical results from the present model are compared to experimental and numerical reference data. Overall, relatively small deviations between the present numerical data and the reference data can be observed. The numerical reference shows good agreement with the experimental data for the wave crest in the region $-0.5 \leq z/d \leq 0$. This good match can also be observed for the present implementation. Towards the bottom boundary, in the region $-0.9 \leq z/d \leq -0.75$, larger deviations between the reference data (numerical and experimental) and the present study can be seen.

For the wave trough, the present implementation, again, shows good agreement with the experimental and numerical reference data at the top of the water column, $-0.5 \leq z/d \leq 0$. It is noteworthy that the behaviour close to the free surface ($-0.1 \leq z/d \leq 0$) is captured well using the present implementation. Towards the bottom boundary, the current implementation shows deviations to the experimental data, but nevertheless provides a better fit than the numerical reference. In the light of the current-only verification case, the deviations close to the bottom boundary are expected and further analysis is required to determine the source of the error.

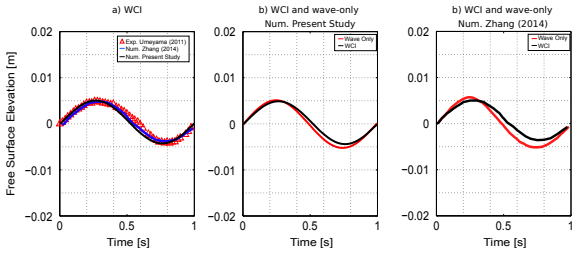

Figure 8: Free surface elevation for the WCI tests case, comparing experimental data (Δ) [16], numerical data by Zhang et al. [2] and numerical results from the present study

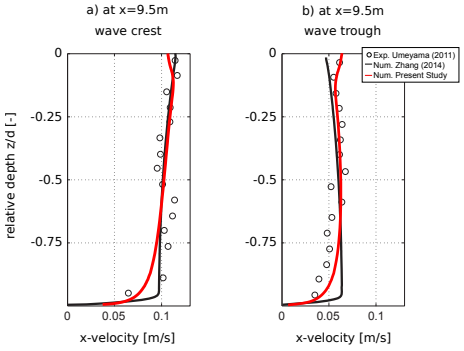

Figure 9: Horizontal x-velocities for the wave only tests case, comparing experimental data (o) [16], numerical data by Zhang et al. [2] and numerical results from the present study

5 CONCLUSION

To simultaneously generate waves and currents in a numerical wave tank, an impulse–source–based approach has been presented. From the verification study, using numerical and experimental reference data, the following conclusions can be drawn:

- The impulse source wavemaker is able to accurately create the desired wave field
- The tank layout effectively shields the current generation area from wave action
- Generated currents can pass through the numerical beaches
- Further work is required to recreate flow profiles accurately, especially close to the bottom boundary
- Despite some remaining issues with current generation, the tendency of decreasing wave height and phase shift for waves travelling in current direction is captured correctly and the presented method is a promising tool to simulate WCI.

Acknowledgement

This paper is based upon work supported by Science Foundation Ireland under Grant No. 13/IA/1886. Pál Schmitt was supported by funding from the European Union Horizon 2020 research and innovation program under grant agreement No 654438.

REFERENCES

[1] M. J. Teles and A. A. Pires-Silva and M. Benoit, Numerical modelling of wave current interactions at a local scale. *Ocean Modelling*, Vol. **68**, pp. 72 – 87, 2013

[2] J.-S. Zhang and Y. Zhang and D.-S. Jeng and P.l.-F. Liu and C. Zhang, Numerical simulation of wave-current interaction using a RANS solver. *Ocean Engineering*, Vol. **75**, pp. 157–164, 2014

[3] M.S. Longuet-Higgins and R.W. Stewart, Changes in the form of short gravity waves on long waves and tidal currents. *Journal of Fluid Mechanics*, Vol. **8**, pp. 565–583, 1960

[4] B. Gaurier and P. Davies and A. Deuff and G. Germain, Flume tank characterization of marine current turbine blade behaviour under current and wave loading. *Renewable Energy*, Vol. **59**, pp. 1–12, 2013

[5] T.A. de Jesus Henriques and S.C. Tedds and A. Botsari and G. Najafian and T.S. Hedges and C.J. Sutcliffe and I. Owen and R.J. Poolem The effects of wave-current interaction on the performance of a model horizontal axis tidal turbine. *International Journal of Marine Energy*, Vol. **8**, pp. 17–35, 2014

[6] E. Fernandez-Rodriguez and T.J. Stallard and P.K. Stansby, Experimental study of extreme thrust on a tidal stream rotor due to turbulent flow with opposing waves. *Journal of Fluids and Structures*, Vol. **51**, pp. 354–361, 2014

[7] S. Ordonez-Sanchez and K. Porter and C. Frost and M. Allmark and C. Johnstone and T. O'Doherty, Effects of Wave-Current Interactions on the Performance of Tidal Stream Turbines. *In Proceedings of the 3rd Asian Wave and Tidal Energy Conference 2016*, 2016

[8] S. Draycott and D. Sutherland and J. Steynor and B. Sellar and V. Venugopal, Re-Creating Waves in Large Currents for Tidal Energy Applications. *Energies*, Vol. **10**, 2017

[9] J.-C. Park and M.-H. Kim and H. Miyata, Three-dimensional numerical wave tank simulations on fully nonlinear wave-current-body interactions. *Journal of Marine Science and Technology*, Vol **6**, pp. 70 – 82, 2001

[10] T. Li and P. Troch and J. De Rouck, Interaction of breaking waves with a current over cut cells. *Journal of Computational Physics*, Vol. **223**, pp. 865 – 897, 2007

[11] D. Markus and R. Wüchner and K.-U. Bletzinger, A numerical investigation of combined wave-current loads on tidal stream generators. *Ocean Engineering*, Vol. **72**, pp. 416 – 428, 2013

[12] S. Tatum and M. Allmark and C. Frost and D. O'Doherty and A. Mason-Jones and T. O'Doherty, CFD modelling of a tidal stram turbine subjected to profiled flow and surface gravity waves. *International Journal of Marine Energy*, Vol. **15**, pp. 156 – 174, 2016

[13] S.-Y. Kim and K.-Y. Kim and J.-C. Park and G.-M. Jeon and H.-H. Chun, Numerical simulation of wave and current interaction with a fixed offshore structure. *International Journal of Naval Architecture and Ocean Engineering*, Vol. **8**, pp. 188–197, 2016

[14] P. Schmitt and C. Windt and J. Davidson and J.V. Ringwood and T. Whittaker, The efficient application of an Impulse Source wave maker to CFD simulations. Submitted to *Coastal Engineering*, 2018

[15] P. Schmitt and B. Elsäßer, A review of wave makers for 3D numerical simulations. *In Proceedings of the MARINE 2015 - Computational Methods in Marine Engineering VI Conference*, pp. 437–446, 2015

[16] M. Umeyama, Coupled PIV and PTV measurements of particle velocities and trajectories for surface waves following a steady current. *Journal of Waterway, Port, Coastal and Ocean Engineering*, Vol. **127**, pp. 85 – 94, 2011

[17] M. Umeyama, Reynolds stresses and velocity distributions in a wave-currents coexisting environment. *Journal of Waterway, Port, Coastal and Ocean Engineering*, Vol. **131**, pp. 203 – 2012, 2005

[18] G. Klopman, Vertical structure of the flow due to waves and currents: laser-Doppler flow measurements for waves following or opposing a current. *Progress Report H840.30 Part II, Delft Hydraulics*, 194

[19] R. Perić and M. Abdel-Maksoud, Analytical prediction of reflection coefficients for wave absorbing layers in flow simulations of regular free-surface waves. *Ocean Engineering*, Vol. **147**, pp. 132–147

[20] C. Windt and J. Davidson and P. Schmitt and J.V. Ringwood, A benchmark study for numerical wavemakers in Computational Fluid Dynamics simulations. *submitted to Coastal Engineering*, 2018